

Supporting information for

Tuning the Reactivity of Ethylene Oligomerization by HZSM-5 Framework Al_f Proximity

Genwei Chen,^{†, a} Hua Liu,^{†, b} Siavash Fadaeerayeni,^a Junjun Shan,^c Aihua Xing,^b Jihong Cheng,^c
Hui Wang,^{*, c} Yizhi Xiang^{*, a}

a. Dave C. Swalm School of Chemical Engineering, Mississippi State University, Mississippi
State, MS, 39762, USA

b. National Institute of Clean-and-Low-Carbon Energy, Beijing 102211, P. R. China

c. NICE America Research, Inc., Mountain View, California 94043, USA

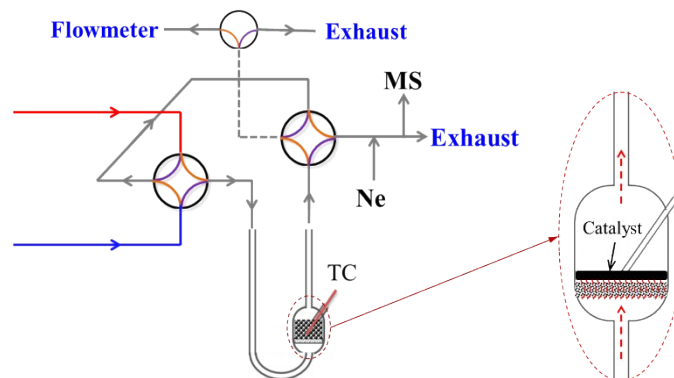


Figure S1. Schematic of the reactor and gas manifold setup used in this study.

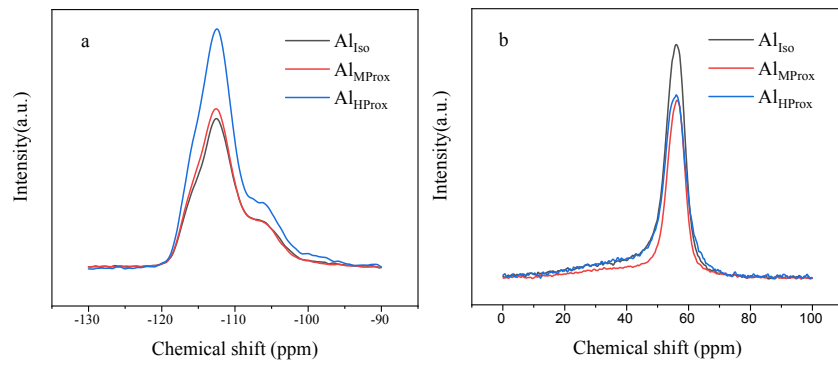


Figure S2. (a) ^{29}Si MAS NMR, (b) ^{27}Al MAS NMR

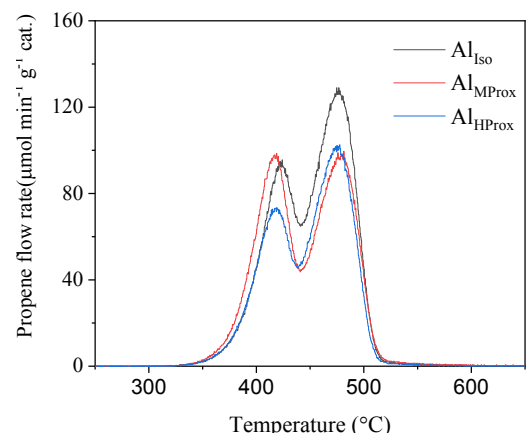


Figure S3. n-propylamine-TPDec profiles

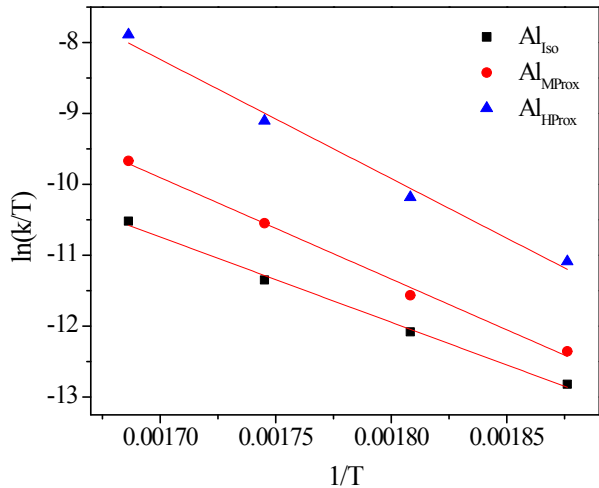


Figure S4. The Eyring plot between $\ln(k/T)$ and $1/T$

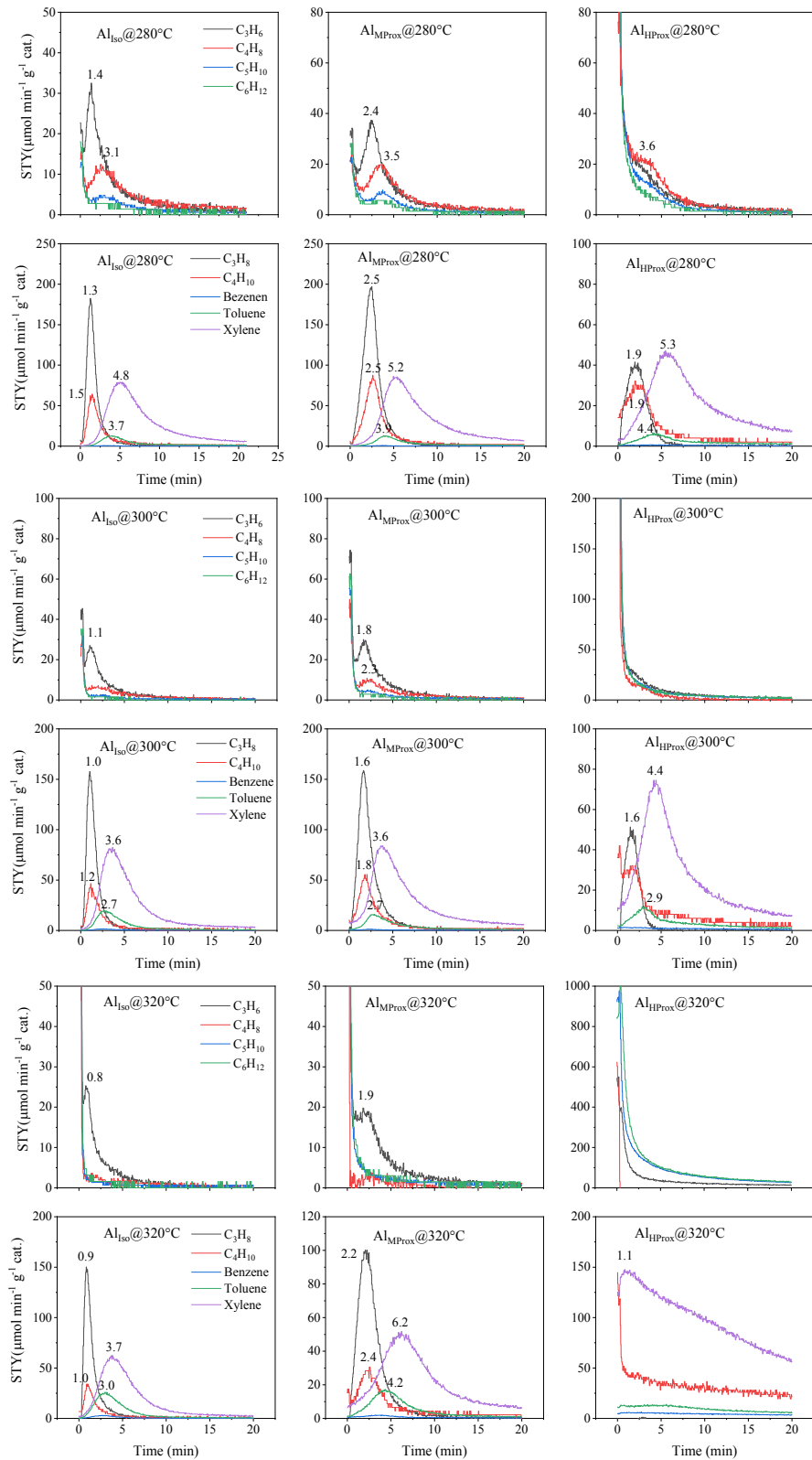


Figure S5. Back transient studies on those three catalysts at 280°C, 300°C and 320°C, respectively.

Table S1. Compilation of catalytic performance data for the heterogeneous ethylene oligomerization from the literature.

Catalyst	Wt. (g)	Flow (ml/min)	T (°C)	Partial pressure	Conversion %	Selectivity /%				Ref.
						C ₃ =	C ₄ =	Alkanes	Aromatics	
H-ZSM-5 (37)	0.5	30	550	30 kPa	81.8	22.9	10.2	31.4	29.2	¹
H-ZSM-5 (11.2)	0.2	20	400	50 kPa	57.2	40.1	21.5	28.3	20.1	²
H-ZSM-5 (38)	0.1	50	300	10.1 kPa	24.2	27.2	27.9	11.2	12.6	³
H-ZSM-5 (78)	0.1	50	450	10.1 kPa	39.6	46.7	22.1	23.9	7.3	³
H-ZSM-5 (23.8)	W/F=3.6g·h/mol		350	33.8 kPa	85.4	15.5	22.3	40.2	4.6	⁴
SSZ-13(Na)	WHSV=0.83h ⁻¹		410	1 atm	40	~81		~19		⁵
SSZ-13(Na)	WHSV=0.83h ⁻¹		410	1 atm	65	~65		~35		⁵
Ni-MCM-41	0.5	16.7	375	9.4 kPa	27	35	62			⁶
ZSM-5	0.55	35	500	1.35 bar	90	22.2	8.8	36.5	10.4	⁷
1K/ZSM-5	0.55	35	500	1.35 bar	87.3	27.3	14.9	30.6	4.1	⁷
ST-ZSM-5	0.55	35	500	1.35 bar	95.1	16.8	10.1	40.8	12.3	⁷
1P/ZSM-5	0.55	35	500	1.35 bar	89.8	23.5	9.4	42	7.5	⁷
H-ZSM-35	0.2	20	400	25 kPa	~40	37.5	32.5			⁸
H-UZM35(0.05)	0.2	20	400	25 kPa	~70	31.4	22.9			⁸
H-UZM35(0.10)	0.2	20	400	25 kPa	~70	28.6	21.4			⁸
H-UZM35(1.0)	0.2	20	400	25 kPa	~40	40	32.5			⁸
SSZ-13(30)	GHSV=0.6L/g/h		400	1atm	~30	~90				⁹
Ni(II)-MCM-41	GHSV=0.2L/g/h		350	1.6 atm	~12	~23	~74	~3		¹⁰
Cr-CoO _x /N-C	WHSV=65.2h ⁻¹		80	13.4 bar	8.6	87.4				¹¹

Table S2. Influence of internal diffusion evaluation according to the Weisz-Prater criterion (Φ_{WP})

Catalyst	T (K)	Rate (mol/g/s)	C_s^* (mol/m ³)	$\Phi_{WP}^{#1}$	$\Phi_{WP}^{#2}$	$\Phi_{WP}^{#3}$
Al _{Iso}	533	1.44E-06	20.58	0.0021	0.01	0.11
Al _{Iso}	553	3.13E-06	19.83	0.0047	0.02	0.24
Al _{Iso}	573	6.75E-06	19.14	0.0106	0.05	0.53
Al _{Iso}	593	1.6E-05	18.50	0.0259	0.13	1.30
Al _{MProx}	533	2.06E-06	20.58	0.0030	0.01	0.15
Al _{MProx}	553	4.71E-06	19.83	0.0071	0.04	0.36
Al _{MProx}	573	1.35E-05	19.14	0.0211	0.11	1.06
Al _{MProx}	593	3.36E-05	18.50	0.0545	0.27	2.72
Al _{HProx}	533	6.52E-06	20.58	0.0095	0.05	0.48
Al _{HProx}	553	1.67E-05	19.83	0.0253	0.13	1.26
Al _{HProx}	573	5.09E-05	19.14	0.0797	0.40	3.99
Al _{HProx}	593	0.000178	18.50	0.2879	1.44	14.40

* C_s is the surface concentration of ethylene, which we assume is similar to the bulk concentration.

Assume ideal gas behavior:

$$C_s \approx C_b = \frac{n}{V} = \frac{P}{RT}$$

The Weisz-Prater number (Φ_{WP}) was calculated for ethylene, based on the first-order reaction.¹²

$$\Phi_{WP} = \eta\varphi^2 = \frac{\text{Rate} \times \rho \times r^2}{C_s D_{eff}}$$

Where ρ is the solid catalyst density (1200 kg/m³), r is the crystal size (1.5 μm), and D_{eff} is the effective diffusivity of ethylene in the zeolite. Since the intracrystal diffusion of ethylene and products is known as “configurational diffusion”, the effective diffusivity is range from 10⁻⁹ to 10⁻¹² m²/s (beyond the Knudsen diffusion).¹³ According to literature, $D_{eff} = 5*10^{-11}$, $1*10^{-11}$, and $1*10^{-12}$ m²/s was selected for calculation, and the results are noted with #¹, #², and #³, respectively.

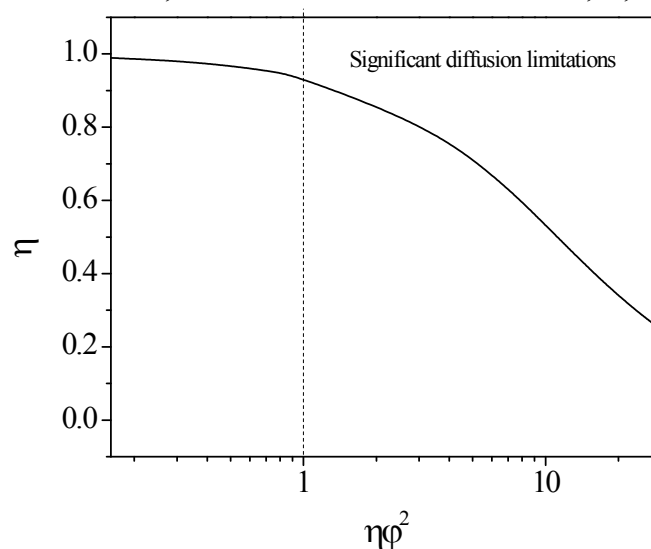


Figure S6. The characteristic function of η vs. $\eta\varphi^2$ (Weisz-Prater number, Φ_{WP}), derived for the sphere crystals and for the first-order reaction.¹² η is the effectiveness factor, φ is the Thiele modulus. It must be noted that, due to the lack of the precise value of effective diffusivity (D_{eff}), the present calculation only provides a rough estimation of the influence of internal diffusion based on the assumption of first-order reaction and sphere crystals. According to Weisz and Prater,¹² the impact of reaction order and the particle shapes on the Φ_{WP} value is not significant in contrast to the D_{eff} .

As we can see from Table S3 and Figure S6, it might be safe to conclude that only a slight diffusion limitation was involved at low reaction temperatures. However, at higher temperatures, the influence of internal diffusion might be significant. For example, the Al_{HProx} sample at 573 and 593 K shows the Weisz-Prater number of 4 and 14.4 (when assuming $D_{eff} = 1*10^{-12}$ m²/s), which corresponds to the effectiveness factor of 0.76 and 0.43, respectively. Nevertheless, the real diffusion limitation must be less significant as estimated with $D_{eff} = 1*10^{-12}$ m²/s. As identified by N₂-physisorption characterization, the Al_{HProx} shows higher mesoporosity than the other two samples, which definitely increased the effective diffusivity (D_{eff}). Based on the molecular dynamics simulation, D_{eff} value for ethylene in MFI zeolite was found $\square 2*10^{-9}$ m²/s at 300 K,¹⁴ and $\square 1.7*10^{-8}$ m²/s at 673 K.¹⁵ As we can see from Table S3, even when applying $D_{eff} = 1*10^{-11}$ and $5*10^{-11}$ m²/s for the calculation, only slight diffusion limitation was expected. Of course, the present study involves higher ethylene concentration, which, as a result, increased the influence of reaction order on the Thiele modulus (the correct reaction order is likely >1).

$$\varphi^2 = \frac{kr^2 C_s^{n-1}}{D_{eff}}$$

However, consider the relatively low Weisz-Prater number shown in Table S3, as well as the true D_{eff} most probably lower than that we employed for calculation, we suggested that only slight internal diffusion limitation might be involved for the present study. Indeed, the linear Arrhenius plot provides another evidence for only slight diffusion limitation over the Al_{HProx} at 593 K (if the diffusion limitation is significant, the data at higher temperatures should deviate negatively from the linear Arrhenius relationship¹³).

Table S3. Detailed product selectivity at steady-state after 30 min time-on-stream.

	T (°C)	C ₂ H ₆	C ₃ H ₈	C ₃ H ₆	C ₄ H ₁₀	C ₄ H ₈	C ₅ H ₁₀	C ₆ H ₁₂	B	T	X
Al _{Iso}	260	0.8	6.2	18.4	6.9	19.7	18.0	27.9	0.2	0.2	1.6
	280	0.2	7.2	19.5	5.5	17.9	19.2	28.3	0.2	0.3	1.8
	300	0.5	2.4	19.5	3.5	16.8	20.3	29.0	0.2	0.8	6.8
	320	0.3	1.6	19.1	2.7	17.9	23.6	32.0	0.2	0.4	2.4
Al _{MProx}	260	0.0	2.3	17.1	5.4	20.9	19.0	30.9	0.3	0.6	3.6
	280	0.8	2.2	18.3	4.5	17.4	20.8	30.9	0.3	0.7	4.1
	300	0.4	1.1	14.5	5.5	11.7	18.1	23.9	0.7	1.7	22.5
	320	0.3	0.5	14.9	4.0	14.5	21.9	27.5	0.4	0.9	15.1
Al _{HProx}	260	0.1	0.0	18.1	3.8	16.1	26.2	34.1	0.2	0.2	1.2
	280	0.3	0.4	15.3	3.6	15.4	28.2	34.6	0.2	0.3	1.7
	300	0.2	0.2	12.7	3.8	14.3	29.1	34.1	0.3	0.5	4.9
	320	0.1	2.8	9.7	7.1	14.2	25.9	27.2	0.3	1.6	11.2

Table S4. The maximum rate for the formation of different products during steady-state and the ratio of maximum rate during transient-state to the steady-state

	steady-state rate ($\mu\text{mol}/\text{min/g}_{\text{cat.}}$)			R _{build-up}			R _{back-transient}		
	Al _{Iso}	Al _{MProx}	Al _{HProx}	Al _{Iso}	Al _{MProx}	Al _{HProx}	Al _{Iso}	Al _{MProx}	Al _{HProx}
C ₃ H ₈	3.57	1.87	0.00	1053.0	1360.0	-	35.9	47.7	-
C ₃ H ₆	10.62	14.04	47.19	305.0	172.9	44.8	2.4	1.4	0.9
C ₄ H ₁₀	2.98	3.30	7.38	1803.6	1114.8	483.7	18.7	14.4	3.3
C ₄ H ₈	8.52	12.89	31.56	285.5	115.7	55.4	1.8	1.1	1.0
C ₅ H ₁₀	6.23	9.39	41.07	208.7	75.4	28.0	1.5	0.9	0.9
C ₆ H ₁₂	8.06	12.73	44.46	102.6	38.8	19.8	1.6	0.9	0.9
Benzene	0.07	0.13	0.20	23.3	3.1	7.1	8.3	3.0	2.2
Toluene	0.06	0.21	0.25	59.4	0.9	8.6	97.9	22.8	12.2
Xylene	0.35	1.10	1.15	11.8	1.5	1.8	99.7	29.6	16.1

The reaction was performed at 260°C and the steady-state rate was collected after TOS 30min

R_{build-up}: ratio of maximum rate of build-up to the steady-state rate

R_{back-transient}, ratio of maximum rate of back-transient to the steady-state rate

Reference

1. S. Follmann and S. Ernst, *New J. Chem.*, 2016, **40**, 4414-4419.
2. W. Dai, X. Sun, B. Tang, G. Wu, L. Li, N. Guan and M. Hunger, *J. Catal.*, 2014, **314**, 10-20.
3. B. Lin, Q. Zhang and Y. Wang, *Ind. Eng. Chem. Res.*, 2009, **48**, 10788-10795.
4. T. Baba, Y. Abe, K. Nomoto, K. Inazu, T. Echizen, A. Ishikawa and K. Murai, *J. Phys. Chem. B*, 2005, **109**, 4263-4268.
5. B. N. Bhadra, J. Y. Song, N. A. Khan, J. W. Jun, T.-W. Kim, C.-U. Kim and S. H. Jhung, *J. Catal.*, 2018, **365**, 94-104.
6. T. Lehmann, T. Wolff, V. M. Zahn, P. Veit, C. Hamel and A. Seidel-Morgenstern, *Catal. Commun.*, 2011, **12**, 368-374.
7. E. Epelde, A. T. Aguayo, M. Olazar, J. Bilbao and A. G. Gayubo, *Appl. Catal. A: Gen.*, 2014, **479**, 17-25.
8. K. Lee, S. H. Cha and S. B. Hong, *ACS Catal.*, 2016, **6**, 3870-3874.
9. J.-W. Jun, N. A. Khan, P. W. Seo, C.-U. Kim, H. J. Kim and S. H. Jhung, *Chem. Eng. J.*, 2016, **303**, 667-674.
10. I. B. Moroz, A. Lund, M. Kaushik, L. Severy, D. Gajan, A. Fedorov, A. Lesage and C. Copéret, *ACS Catal.*, 2019, **9**, 7476-7485.
11. Z. Xu, J. P. Chada, L. Xu, D. Zhao, D. C. Rosenfeld, J. L. Rogers, I. Hermans, M. Mavrikakis and G. W. Huber, *ACS Catal.*, 2018, **8**, 2488-2497.
12. D. M. Ruthven and M. F. M. Post, in *Studies in Surface Science and Catalysis*, eds. H. van Bekkum, E. M. Flanigen, P. A. Jacobs and J. C. Jansen, Elsevier, 2001, vol. 137, pp. 525-577
13. P. B. Weisz and C. D. Prater, in *Advances in Catalysis*, eds. W. G. Frankenburg, V. I. Komarewsky and E. K. Rideal, Academic Press, 1954, vol. 6, pp. 143-196.
14. F. Jianfen, B. van de Graaf, H. M. Xiao and S. L. Njo, *J. Mol. Struc-Theochem*, 1999, **492**, 133-142.
15. C. Wang, B. Li, Y. Wang and Z. Xie, *J. Energy Chem.*, 2013, **22**, 914-918